Journal of Pharmaceutical Analysis 10 (2020) 490–497

Contents lists available at ScienceDirect

Journal of Pharmaceutical Analysis

journal homepage: www.elsevier.com/locate/jpa

Short communication

A pyrene-based ratiometric fluorescent probe with a large Stokes shift for selective detection of hydrogen peroxide in living cells

Qingxin Chen [a, b], Ke Cheng [a, b], Wanhe Wang [a, b], Liu Yang [a, c], Yusheng Xie [a, b], Ling Feng [a, b], Jie Zhang [a, c], Huatang Zhang [d], Hongyan Sun [a, c, *]

[a] Department of Chemistry and Center of Super-Diamond and Advanced Films, City University of Hong Kong, Hong Kong, China
[b] Key Laboratory of Biochip Technology, Biotech and Health Centre, City University of Hong Kong Shenzhen Research Institute, Shenzhen, 518057, China
[c] Chengdu Research Institute, City University of Hong Kong, Chengdu, 610000, China
[d] School of Chemical Engineering and Light Industry, School of Biomedical and Pharmaceutical Sciences, Guangdong University of Technology, Guangzhou, 510006, China

ARTICLE INFO

Article history:
Received 31 January 2020
Received in revised form
12 July 2020
Accepted 15 July 2020
Available online 4 August 2020

Keywords:
Hydrogen peroxide
Fluorescent probe
Pyrene
Ratiometric detection
Large Stokes shift

ABSTRACT

Hydrogen peroxide (H_2O_2) plays a significant role in regulating a variety of biological processes. Dysregulation of H_2O_2 can lead to various diseases. Although numerous fluorescent imaging probes for H_2O_2 have been reported, the development of H_2O_2 ratiometric fluorescent probe with large Stokes shift remains rather limited. Such probes have shown distinct advantages, such as minimized interference from environment and improved signal-to noise ratio. In this work, we reported a new pyrene-based compound **Py-VPB** as H_2O_2 fluorescent probe in vitro. The probe demonstrated ratiometric detection behavior, large Stokes shift and large emission shift. In addition, the probe showed high sensitivity and selectivity towards H_2O_2 in vitro. Based on these excellent properties, we successfully applied **Py-VPB** to the visualization of exogenous and endogenous H_2O_2 in living cells. Cell imaging study also showed that our probe was localized in the mitochondria. We envision that the probe can provide a useful tool for unmasking the biological roles of mitochondrial H_2O_2 in living systems.

1. Introduction

Hydrogen peroxide (H_2O_2), one of the major reactive oxygen species (ROS), plays a crucial role in regulating various biological processes, including cell growth [1], proliferation, apoptosis [2], and signaling pathways [3]. Aberrant generation and accumulation of H_2O_2, on the other hand, can lead to damages of DNA [4], RNA [5] and protein [6], potentially causing various diseases such as cardiovascular diseases [7], Alzheimer's disease [8], and cancer [9,10]. Therefore, a methodology that can detect H_2O_2 level in living biological system is of great importance. To date, various analytical methods have been established to detect H_2O_2, such as electrochemical methods, colorimetry, chromatography and spectroscopy. Most of these methods, however, suffer from tedious sample preparation and manipulation procedures, as well as disruption of cells and tissue structures [11–14]. As a result, these methods are not suitable for detecting H_2O_2 in living systems. It therefore, calls for the development of new chemical tools to unmask the biological roles of H_2O_2 in vitro and in vivo.

Fluorescent imaging has become an attractive method for detecting various biomolecules due to its advantages of non-invasiveness, high sensitivity, real-time monitoring ability as well as high spatiotemporal resolution [15–21]. Due to the prominent properties of fluorescence-based methods, increasing varieties of fluorescent probes have been developed for detecting and imaging H_2O_2 [22–34]. Unfortunately, most of these probes suffer from problems such as single channel output or small Stokes shift, which considerably hinders their applications in biological imaging. For example, it is well known that single channel fluorescent probes, which only rely on the change of fluorescence intensity in a single channel, are susceptible to various interferences from instruments or environments, such as changes in probe concentration, pH, local environment polarity and laser excitation power [35]. In contrast, ratiometric fluorescent probes, which have two emission bands, can effectively alleviate the aforementioned interferences owing to

Peer review under responsibility of Xi'an Jiaotong University.
* Corresponding author. Department of Chemistry and Center of Super-Diamond and Advanced Films (COSDAF), City University of Hong Kong, Hong Kong, China.
E-mail address: hongysun@cityu.edu.hk (H. Sun).

https://doi.org/10.1016/j.jpha.2020.07.003

their self-calibration function [36–41]. The existing ratiometric fluorescent probes for H_2O_2, however, are limited by low aqueous solubility and small Stokes shift. Fluorescent probes with small Stokes shift have several disadvantages, such as self-quenching effect and interference from excited light and scattered light, etc. In contrast, fluorescent probes with large Stokes shift are capable of minimizing the crosstalk between excitation and emission light, thereby greatly increasing the signal-to-noise ratio. Consequently, the development of new ratiometric fluorescent probes with large Stokes shift for detecting H_2O_2 will be highly desired to increase the sensitivity and precision of the probe.

Pyrene-based fluorescent probes have received sustained attention in recent years due to their ratiometric flourescence behavior and high quantum yield. The desirable photophysical properties of pyrene-type dyes prompted us to develop pyrene-based H_2O_2 probe. In this work, we introduced a well-known H_2O_2 responsive unit (aryl boric acid ester) into a pyrene-based fluorophore to serve as a ratiometric fluorescent probe for detecting H_2O_2. The designed probe was shown to be capable of sensitively and selectively detecting H_2O_2 in aqueous solution with large Stokes shift. Furthermore, the probe was demonstrated to be a mitochondria-targeted probe and successfully applied to visualize exogenous and endogenous H_2O_2 in living cells (Scheme 1).

2. Experimental

2.1. Materials and methods

Pyrene-1-carbaldehyde was purchased from J&K (Beijing, China). All the other reagents were of analytical reagent grade and used as received without further purification. Cell culture related items, including fetal bovine serum (FBS), Dulbecco's modified Eagle's medium (DMEM), trypsin-EDTA, PBS, and penicillin/streptomycin, were purchased from Invitrogen. Water used in all experiments was distilled twice and refined by a Milli-Q system (Millipore, USA). 8-well of ibidi® culture plates were purchased from ibidi GmbH for imaging purpose.

NMR spectra were recorded on a Bruker 300 MHz NMR spectrometer. UV absorption spectra of **Py-VPB** and **Py-VP** were measured on Shimadzu 1700 UV/Vis Spectrometer. Fluorescence emission spectra of **Py-VPB** and **Py-VP** were taken on a FluoroMax-4 fluorescence photometer. Mass spectra of compounds were acquired using a PC Sciex API 150 EX ESI-MS system. Fluorescence images of HeLa cells were recorded with a Leica TCS SPE confocal scanning microscope. pH values of different buffers were measured with a FiveEasy TM Fe20 pH meter.

2.2. Synthesis of Probe *Py-VPB*

Probe **Py-VPB** was synthesized as shown in Scheme 2.

2.2.1. Synthesis of *Py-VP*

Pyrene-1-carbaldehyde (230 mg, 1.0 mmol) and 4-methylpyridine (466 mg, 5.0 mmol) were dissolved in Ac_2O (10 mL) and purged with N_2. The mixture was then stirred overnight under reflux. After reaction, the mixture was cooled to room temperature and 5% NaOH aqueous solution was added. After being stirred for 10 min, the solution was extracted twice with ethyl acetate. The organic phase was combined and dried with anhydrous Na_2SO_4. The solvent was then evaporated, and the crude product was purified by column chromatography (n-hexane/ethyl acetate 10:1 to 2:1) to provide a yellowish powder (206 mg, 67.5%). ^{1}H NMR (300 MHz, d_6-DMSO) δ 8.82 (d, J = 9.4 Hz, 1H), 8.71 (d, J = 16.1 Hz, 1H), 8.63 (d, J = 5.9 Hz, 2H), 8.56 (d, J = 8.2 Hz, 1H), 8.32 (dd, J = 12.9, 8.5 Hz, 4H), 8.21 (s, 2H), 8.09 (t, J = 7.6 Hz, 1H), 7.87 (d, J = 6.1 Hz, 2H), 7.57 (d, J = 16.1 Hz, 1H). ^{13}C NMR (75 MHz, d_6-DMSO) δ 150.48, 144.98, 131.47, 131.45, 130.90, 130.88, 129.91, 129.50, 128.81, 128.36, 128.20, 127.87, 126.93, 126.12, 125.86, 125.80, 124.69, 124.45, 124.24, 123.73, 121.78. ESI-MS m/z calcd for $[M+H]^+$ 306.1, found 306.2.

2.2.2. Synthesis of *Py-VPB*

Py-VP (46 mg, 0.15 mmol) and 1-(4-(bromomethyl) phenyl)-3,3,4,4-tetramethylborolane (60 mg, 0.20 mmol) were dissolved in acetonitrile. The mixture was stirred under reflux overnight. After being cooled to room temperature, the precipitate was obtained and centrifuged. The precipitate was washed three times with ethyl ether and dried under vacuum to obtain a tangerine powder (65 mg, 72.4%). ^{1}H NMR (300 MHz, d_6-DMSO) δ 9.20–9.07 (m, 3H), 8.96 (d, J = 9.4 Hz, 1H), 8.67 (d, J = 8.3 Hz, 1H), 8.57 (d, J = 6.7 Hz, 2H), 8.46–8.35 (m, 4H), 8.29 (q, J = 8.9 Hz, 2H), 8.16 (t, J = 7.6 Hz, 1H), 7.88 (d, J = 16.0 Hz, 1H), 7.77 (d, J = 7.9 Hz, 2H), 7.56 (d, J = 8.0 Hz, 2H), 5.84 (s, 2H), 1.30 (s, 12H). ^{13}C NMR (75 MHz, d_6-DMSO) δ 153.77, 144.79, 138.27, 137.81, 135.66, 132.84, 131.33, 130.74, 130.02, 129.41, 129.29, 129.07, 128.49, 127.86, 127.19, 127.12, 126.76, 126.51, 126.05, 125.92, 125.08, 124.74, 124.62, 124.20, 123.61, 84.37, 62.56, 25.11. ESI-MS m/z calcd for $C_{36}H_{33}BNO_2$ $[M]^+$ 522.3, found 522.4.

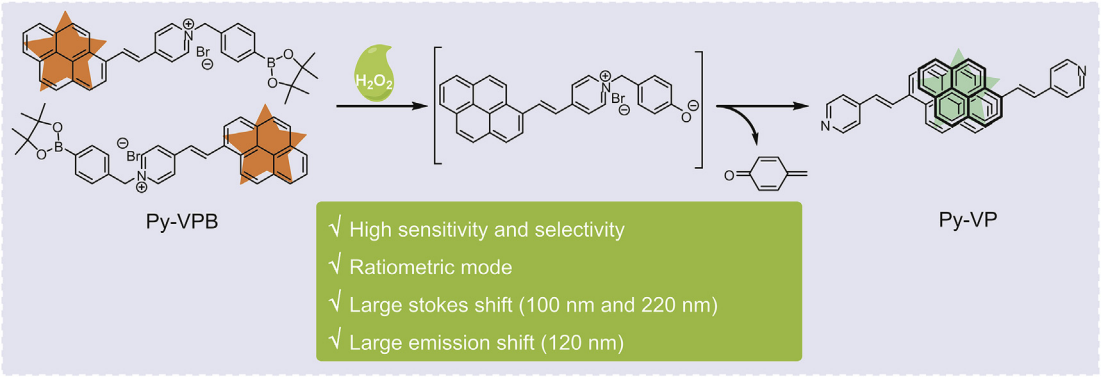

Scheme 1. Schematic diagram of the detection mechanism of the probe **Py-VPB**.

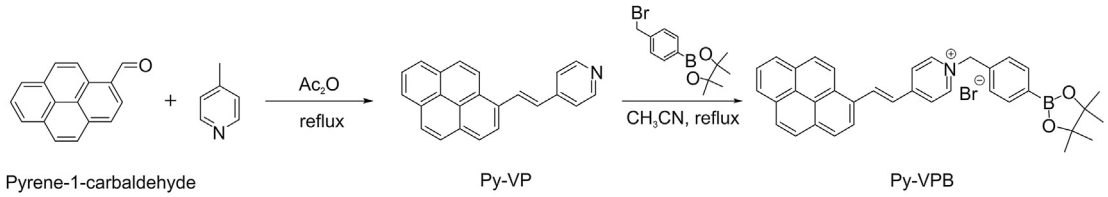

Scheme 2. Synthetic route of probe **Py-VPB** for H_2O_2 detection.

2.3. Spectroscopic measurements

10 mM stock solution of probe **Py-VPB** was prepared in DMSO. H_2O_2 and other biological analytes were prepared in sodium borate buffer (10 mM, pH = 8.5) as 10 mM stock solutions according to the reported literature [42]. All the measurements were taken in sodium borate buffer (10 mM, pH = 8.5) containing 20% DMSO (*V/V*) under 37 °C. The excitation wavelength was set to 380 nm. The emission wavelength was set in the range from 395 nm to 745 nm. The slit widths were set to 5/5 nm.

2.4. CCK8 assay

HeLa cells were seeded into 96-well plates in 100 μL of DMEM supplemented with 10 μL of FBS and 1 μL of penicillin/streptomycin. The cell density was 5×10^3 cells per well. The cells were allowed to grow overnight under an atmosphere of 5% CO_2 at 37 °C. Each well was washed with 100 μL of PBS, and then the cells were treated with various concentrations of **Py-VPB** (0, 5, 10, 20, 50 and 100 μM). The cells were then incubated in the incubator for another 24 h. Subsequently 10 μL of CCK-8 reagent was added. The cells were further cultured for another 2 h. Finally, the absorbance was measured at 450 nm. Cell viability was expressed as a percentage of the control cells.

2.5. Cell culture

HeLa cells were cultured in DMEM supplemented with 1% penicillin/streptomycin and 10% FBS at 37 °C under 5% CO_2. Approximately 10^5 cells were seeded in a confocal dish (35 mm).

2.6. Fluorescence microscope imaging

For exogenous H_2O_2 detection, HeLa cells were incubated with probe **Py-VPB** (10 μM) at 37 °C for 20 min. Subsequently, the cells were washed with DMEM twice to remove excess **Py-VPB**. H_2O_2 (100 μM or 200 μM) was added to the cells and incubated for another 60 min. Cells treated with **Py-VPB** (10 μM) only were used as a negative control.

For endogenous H_2O_2 imaging, RAW 264.7 cells were pretreated with 5 μg/mL phorbol 12-myristate 13-acetate (PMA) for 8 h while cells incubated with DMEM only were used as a negative control. **Py-VPB** (10 μM) was then incubated with both cells for one more hour. For the colocalization experiment, **Py-VPB** (10 μM) and **Mito Tracker™ Red** (100 nM) were co-incubated with HeLa cells for 20 min.

Cell imaging study was conducted using a Leica TCS SPE confocal scanning microscope. Two fluorescence channels were used: Ex: 405 nm, Em: 450–500 nm for channel 1, and 580–630 nm for channel 2.

3. Results and discussion

3.1. Design principle and synthesis of the probe *Py-VPB*

Pyrene-based dyes are widely used as fluorescent probes based on the π-π interactions. Through these interactions, their monomer and excimer states can be regulated by addition of analytes, resulting in fluorescence signal changes [43,44]. This type of signal change generally displays large Stokes shift and ratiometric mode. However, fluorophore pyrene itself is a highly hydrophobic molecule. It has very low aqueous solubility, limiting further biological applications. We herein introduced a quaternary ammonium unit that is linked with H_2O_2 responsive unit into pyrene moiety. By doing so, the positive charge of the probe **Py-VPB** increases its water solubility and prefers the formation of monomer. After reaction with H_2O_2, the probe turned into a neutral molecule **Py-VP**. This increased the reaction product's hydrophobicity and promoted its aggregation to form excimer. During this reaction process, the fluorescence emission peak changed from 600 nm of monomer state to 480 nm of excimer state, thereby achieving ratiometric detection of H_2O_2.

The probe **Py-VPB** was prepared in two steps. Compound **Py-VP** was first synthesized through Knoevenagel condensation between pyrene-1-carbaldehyde and 4-methylpyridine, followed by quaternization reaction to afford the desirable probe **Py-VPB** (Scheme 2). All chemical structures of the synthetic compounds were fully characterized by ^1H, ^{13}C NMR, and ESI–MS spectra (Fig. S1–S6). Subsequently we performed absorption and emission study on **Py-VPB** and **Py-VP**. **Py-VPB** showed two main absorption peaks at 320 nm and 440 nm while **Py-VP** displayed a single absorption peak at 370 nm (Fig. S7A). Meanwhile, the former demonstrated an emission peak at 600 nm while the latter displayed a large blue shift at 480 nm (Fig. S8A). These experimental data demonstrated that **Py-VPB** is a potential ratiometric fluorescent probe with large Stokes shift and emission shift as we expected.

3.2. Fluorescence response of *Py-VPB* towards H_2O_2

With the probe **Py-VPB** in hand, we first examined its fluorescence response towards H_2O_2. As shown in Fig. 1A, when excited at 380 nm, the probe exhibited a main fluorescence peak at 600 nm with a quantum yield (ϕ) of 0.27 (coumarin 120 as a reference) in the absence of H_2O_2. After incubation with 100 μM of H_2O_2 for 30 min, the fluorescence intensity at 600 nm decreased rapidly while an intense emission peak at 480 nm emerged (Fig. S8B–C). It is the characteristic peak of pyrene excimer (quantum yield of 0.52), indicating the formation of pyrene excimer [45]. A maximum of 27-fold fluorescence increase could be observed at the emission wavelength of 480 nm (Fig. S8B). Moreover, the ratio of the fluorescence intensities at 480 and 600 nm (I_{480}/I_{600}) displayed a maximum of 66.5-fold change after the addition of H_2O_2 (Fig. 1B). The fluorescence signal of the probe showed a good linear relationship with H_2O_2 concentration in the range of 0–45 μM. The detection limit (LOD) was determined to be 117 nM according to 3σ/

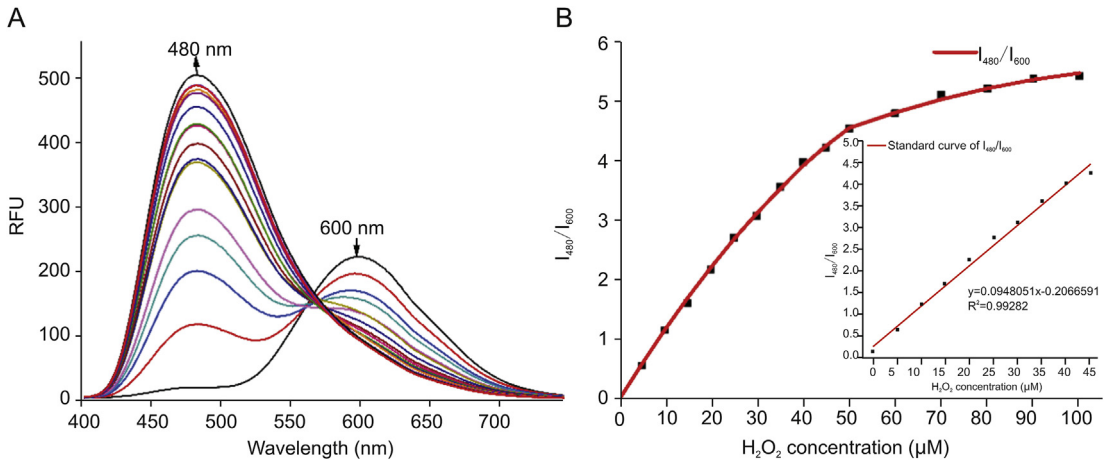

Fig. 1. Quantitative measurements of **Py-VPB** (10 μM) fluorescence changes after addition of different concentrations of H_2O_2. (A) Fluorescence emission spectra of **Py-VPB** after addition of different concentrations of H_2O_2 (0–100 μM). (B) Plot of fluorescence intensity ratio changes (I_{480}/I_{600}) after incubation with increasing amounts of H_2O_2. Inset: Linear regression plot of fluorescence intensity ratio change (I_{480}/I_{600}) as a function of the concentration of H_2O_2 (0–45 μM). Ex = 380 nm.

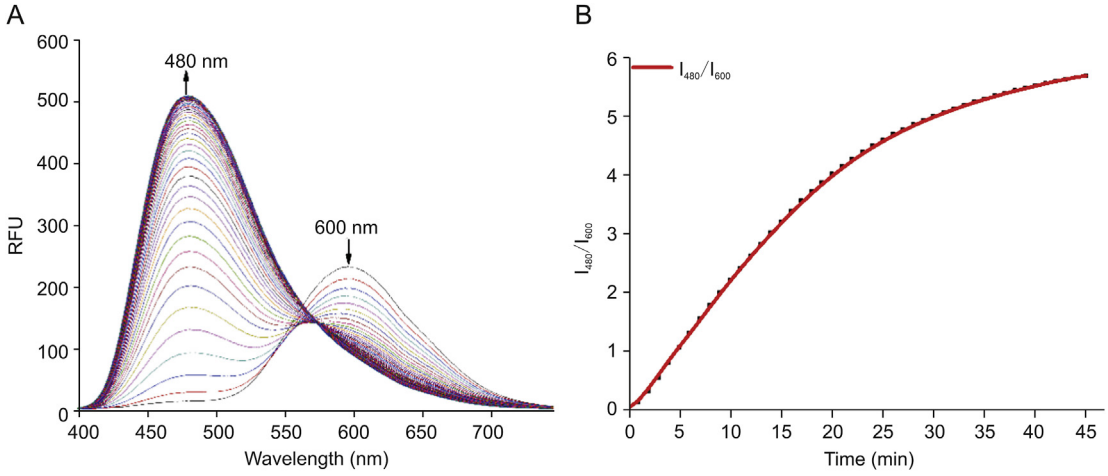

Fig. 2. Time-dependent response of **Py-VPB** to H_2O_2. (A) Fluorescence emission spectra of **Py-VPB** after incubation with 100 μM H_2O_2 for different time intervals (0–45 min). (B) Plot of I_{480}/I_{600} ratio changes after incubation with 100 μM H_2O_2 for different time intervals (0–45 min). Ex = 380 nm.

κ, where σ is the standard deviation of blank measurements and κ is the slope (Fig. 1B). The value is relatively lower than most of the reported H_2O_2 probes [24,27,29,31,46,47] (Table S1).

We further carried out time-dependent experiments of **Py-VPB** with H_2O_2. Kinetic study showed that **Py-VPB** exhibited moderate reaction rate with H_2O_2. As shown in Fig. 2 and Fig. S9, the fluorescence at 480 nm plateaued within 45 min along with the disappearance of the peak at 600 nm in the presence of 100 μM H_2O_2. The effect of pH was also investigated. Results showed that the probe **Py-VPB** responded well to H_2O_2 in alkaline conditions (Fig. S10). Thus **Py-VPB** is suitable for application in biological systems.

To rule out interference from other biological species coexisting in living systems, high selectivity towards H_2O_2 is an essential parameter to ensure the biological applications of the fluorescent probes. Gratifyingly, we observed that **Py-VPB** possessed excellent selectivity toward H_2O_2 over the other common biological interfering species (Fig. 3 and Fig. S11). It is worth noting that the ratio of I_{480}/I_{600} to H_2O_2 was much higher than that of many ROSs including ClO^-, HO· and $O_2^{\cdot-}$. Although $ONOO^-$ showed moderate fluorescence response towards **Py-VPB**, the signal was relatively small

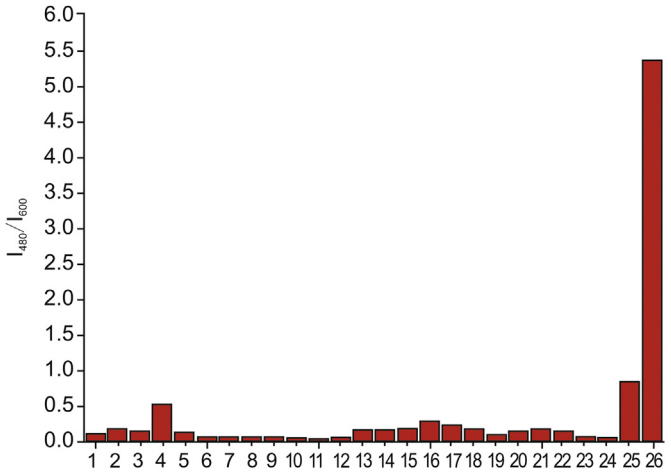

Fig. 3. Relative fluorescence responses of **Py-VPB** (10 μM) to various analytes (100 μM): (1) Blank, (2) Mg^{2+}, (3) Ca^{2+}, (4) Cu^{2+}, (5) Fe^{2+}, (6) Cr^{3+}, (7) Co^{2+}, (8) Zn^{2+}, (9) F^-, (10) Cl^-, (11) I^-, (12) PO_4^{3-}, (13) NO_3^-, (14) NO_2^-, (15) SO_3^{2-}, (16) GSH, (17) Hcy, (18) Cys, (19) ·NO, (20) TBO·, (21) t-BuOOH, (22) ClO^-, (23) HO·, (24) $O_2^{\cdot-}$, (25) $ONOO^-$, (26) H_2O_2.

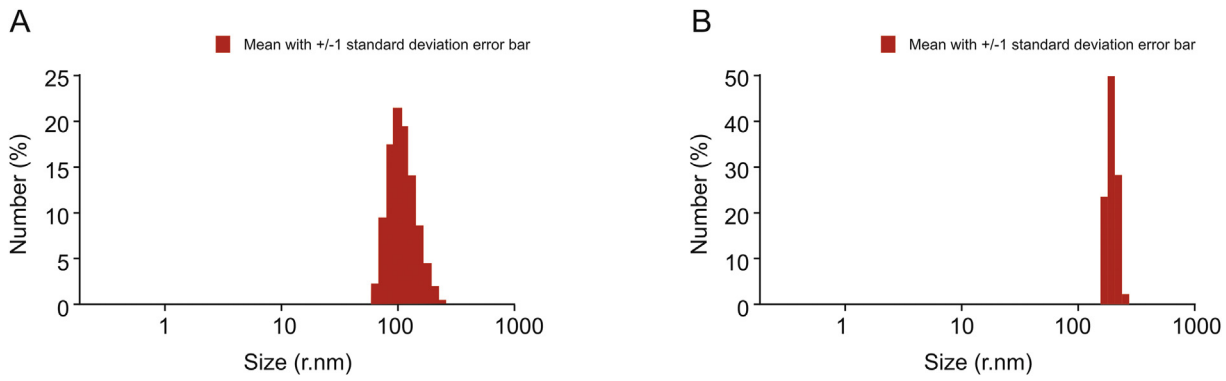

Fig. 4. DLS data of **Py-VPB** (A) and **Py-VP** (B) in water/DMSO (4:1, *V/V*).

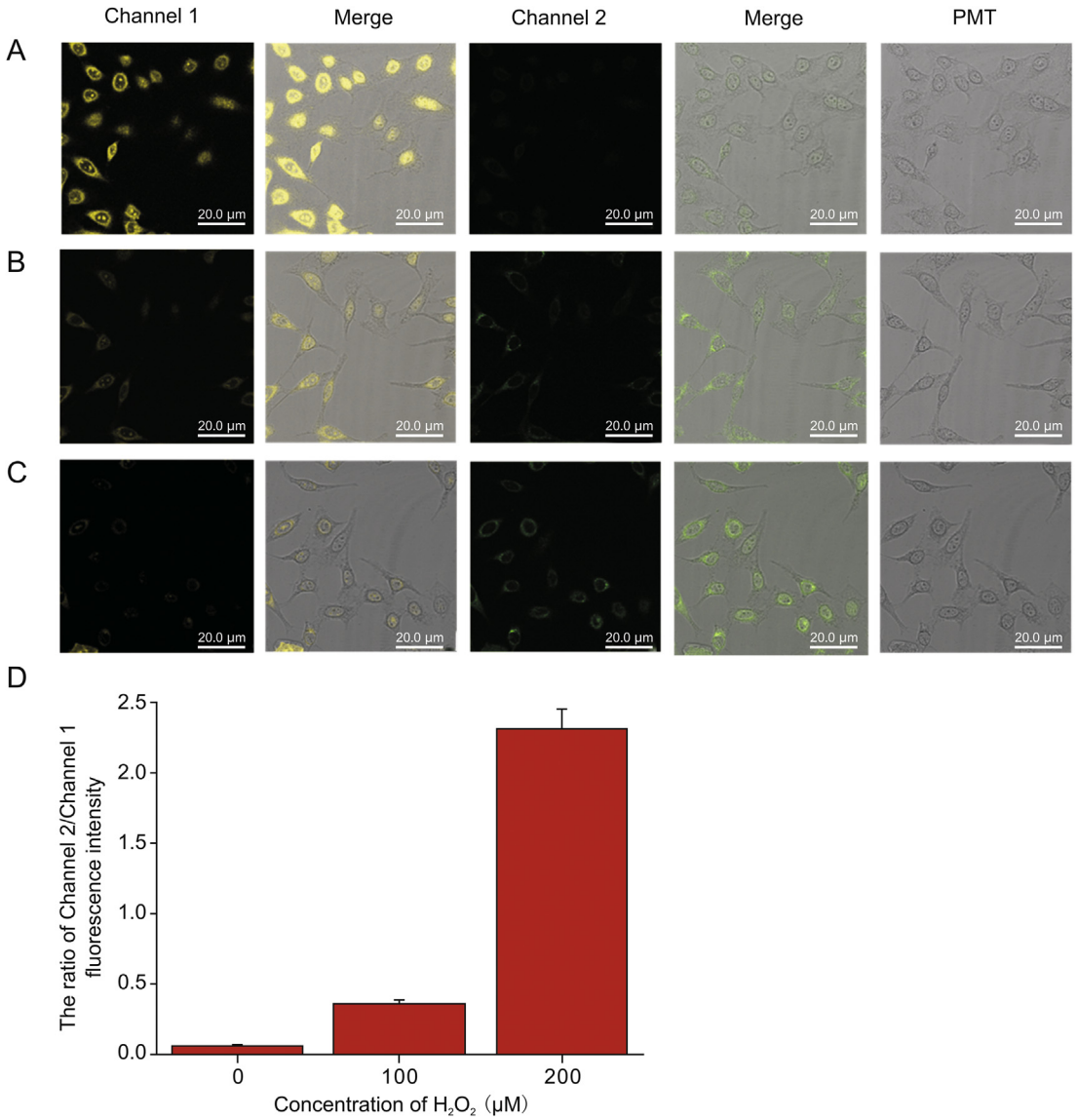

Fig. 5. (A-C) Confocal imaging of exogenous H_2O_2 in HeLa cells (A: 0 μM; B: 100 μM; C: 200 μM). (D) The ratio of channel 2/channel 1 fluorescence intensity when incubated with different concentrations of H_2O_2. The relative fluorescence intensity was analyzed by the ImageJ software. Every data point represents the mean of five fields of cells. Ex = 405 nm, channel 1: 580–630 nm (**Py-VPB**), channel 2: 450–500 nm (**Py-VP**). Scale bar = 20.0 μm.

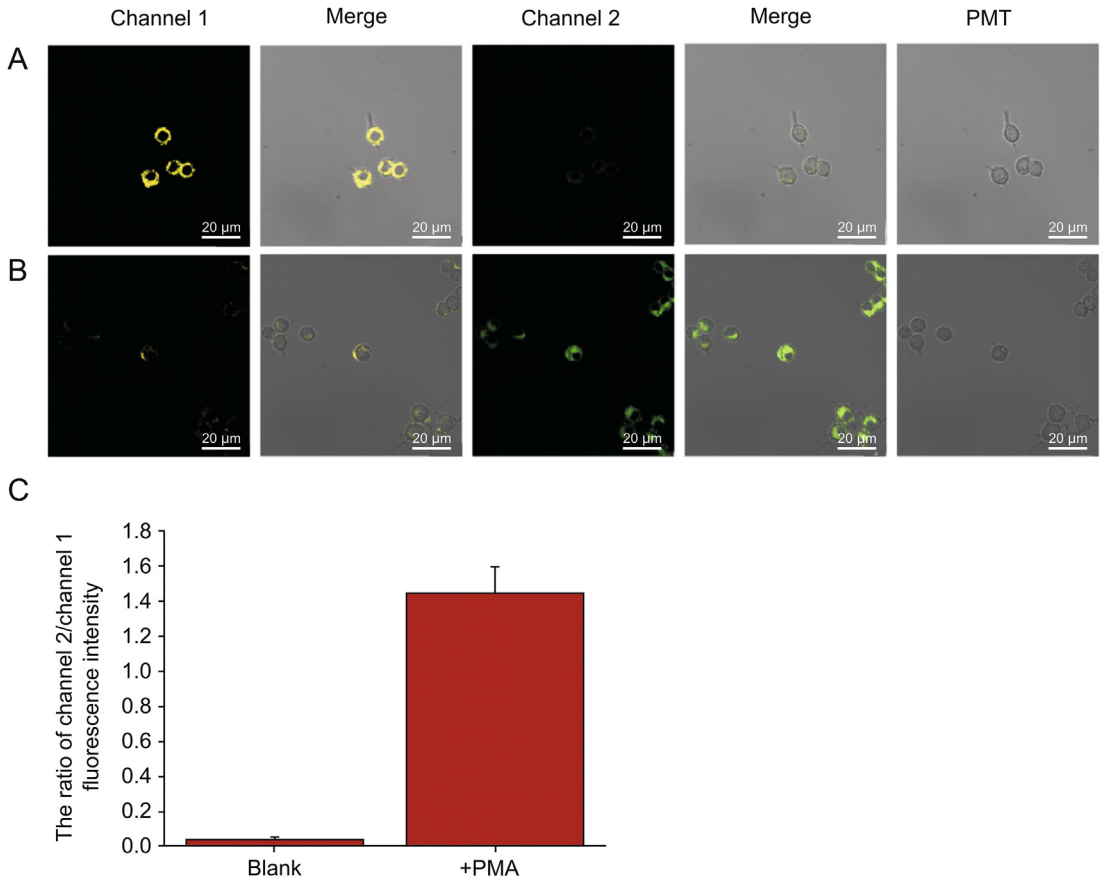

Fig. 6. (A-B) Confocal imaging of endogenous H_2O_2 in RAW264.7 cells (A: blank; B: pretreated with PMA). (C) The ratio of channel 2/channel 1 fluorescence intensity. The relative fluorescence intensity was analyzed by the ImageJ software. Every data point represents the mean of five fields of cells. Ex = 405 nm, channel 1: 580–630 nm (**Py-VPB**), channel 2: 450–500 nm (**Py-VP**). Scale bar = 20.0 μm.

compared with that of H_2O_2, signifying our probe displayed good selectivity in detecting H_2O_2. The results were consistent with those in the recently reported literature [48–50]. This further demonstrated the potential use of our probe in a complex cellular environment.

3.3. Studies of reaction mechanism

Encouraged by the results above, we further verified the reaction mechanism of the probe reacting with H_2O_2. As illustrated in Fig. 1A and Fig. S7, the absorption and fluorescence spectra of **Py-VPB** after incubation with H_2O_2 were identical to those of **Py-VP**, confirming the chemical transformation from **Py-VPB** to **Py-VP**. This result was further supported by the mass spectrometry analysis. In the mass spectrometry results, a peak at m/z 306.2 corresponding to **Py-VP** was observed when **Py-VPB** was treated with H_2O_2 (Fig. S12). We next used dynamic light scattering (DLS) to investigate the size of **Py-VP** and **Py-VPB** in aqueous solution. **Py-VP** was expected to exist in an aggregation state in aqueous solution while **Py-VPB** should stay in a relatively dispersed state. As shown in Fig. 4, the particle size of **Py-VPB** solution containing 80% water fraction was estimated to be 131.4 nm (Fig. 4A). The particle size of **Py-VP**, on the other hand, showed considerable aggregation with an average diameter of 201.9 nm (Fig. 4B). These results indicate that when the positive charge of **Py-VPB** was removed by H_2O_2, the solubility of the resulting **Py-VP** dramatically decreased, thereby inducing the formation of excimer.

3.4. Fluorescence imaging in cells

Prior to applying the probe to cell imaging, the cytotoxicity of **Py-VPB** with HeLa cells was assessed by the CCK8 method [51] (Fig. S13). Results revealed that cell viability was higher than 90% even when the concentration of **Py-VPB** was up to 20 μM, demonstrating that the probe had a low cytotoxicity. Its low cytotoxicity prompted us to detect exogenous H_2O_2 in HeLa cells. As shown in Fig. 5, when the cells were incubated with **Py-VPB** (10 μM), they only showed obvious fluorescence in channel 1 (Fig. 5A) but negligible fluorescence in channel 2 (Fig. 5A). In contrast, with the treatment of H_2O_2, the fluorescence in channel 1 decreased dramatically while the fluorescence in channel 2 was significantly enhanced (Fig. 5B–C), indicating **Py-VPB** could penetrate cell membrane and was capable of visualizing H_2O_2. Moreover, the ratio of channel 2/channel 1 fluorescence intensity increased with the increasing concentration of H_2O_2 in cells (Fig. 5D), suggesting the potential of **Py-VPB** to quantify H_2O_2 in living cells.

To explore the sub-cellular localization of **Py-VPB**, colocalization experiment was carried out with **Py-VPB** and a commercial mitochondrial probe **Mito Tracker™ Red**. As shown in Fig. S14, the signal of **Py-VPB** overlapped well with that of **Mito Tracker™ Red** and the Pearson's correlation coefficient was determined to be 0.92 (Fig. S15), indicating that probe **Py-VPB** was localized in the mitochondria of cells.

Subsequently, **Py-VPB** was employed to visualize endogenous H_2O_2 in RAW264.7 cells. As shown in Fig. 6, RAW264.7 cells stimulated by PMA displayed drastic fluorescence decrease in channel 1.

Meanwhile, fluorescence in channel 2 was considerably enhanced. Through ImageJ analysis, the ratio of channel 2/channel 1 fluorescence intensity was found to increase from 0.04 to 1.44 (Fig. 6C). These results together prove that **Py-VPB** is biocompatible and capable of detecting exogenous and endogenous H_2O_2 in living cells.

4. Conclusions

In summary, we developed a new pyrene-based ratiometric fluorescent probe with a large Stokes shift (100 nm and 220 nm) as well as high sensitivity and selectivity for H_2O_2. In the presence of H_2O_2, the fluorescence of **Py-VPB** underwent a large blue-shift (120 nm), whereby the emission peak at 480 nm emerged while the peak at 600 nm decreased. The ratiometric mode effectively decreased the signal interference from local environment and instrument variation. Moreover, this probe showed a 66.5-fold I_{480}/I_{600} change with a LOD of 117 nM. The probe also displayed low cytotoxicity, mitochondria-targeting ability and it was capable of detecting exogenous and endogenous H_2O_2 in living cells. Taken together, this probe displays several advantageous properties compared with the existing probes, providing a promising tool to explore the roles of H_2O_2 in living systems.

Declaration of competing interest

The authors declare that there are no conflicts of interest.

Acknowledgments

This work was supported by the Science Technology and Innovation Committee of Shenzhen Municipality (JCYJ20180507181654823), the National Natural Science Foundation of China (21778044), and Sichuan Science and Technology Program (2018JY0360).

Appendix A. Supplementary data

Supplementary data to this article can be found online at https://doi.org/10.1016/j.jpha.2020.07.003.

References

[1] R.S. Arnold, J. Shi, E. Murad, et al., Hydrogen peroxide mediates the cell growth and transformation caused by the mitogenic oxidase Nox1, Proc. Natl. Acad. Sci. U.S.A. 98 (2001) 5550–5555.
[2] F. Benetti, J.E. Gomes-Filho, L.L. Ferreira, et al., Hydrogen peroxide induces cell proliferation and apoptosis in pulp of rats after dental bleaching in vivo: effects of the dental bleaching in pulp, Arch. Oral Biol. 81 (2017) 103–109.
[3] S.G. Rhee, H_2O_2, a necessary evil for cell signaling, Science 312 (2006) 1882–1883.
[4] N. Driessens, S. Versteyhe, C. Ghaddhab, et al., Hydrogen peroxide induces DNA single- and double-strand breaks in thyroid cells and is therefore a potential mutagen for this organ, Endocr.-Relat. Cancer. 16 (2009) 845–856.
[5] T. Hofer, C. Badouard, E. Bajak, et al., Hydrogen peroxide causes greater oxidation in cellular RNA than in DNA, Biol. Chem. 386 (2005) 333–337.
[6] A. Poljak, I.W. Dawes, B.A. Ingelse, et al., Oxidative damage to proteins in yeast cells exposed to adaptive levels of H_2O_2, Redox Rep. 8 (2003) 371–377.
[7] C.H. Byon, J.M. Heath, Y. Chen, Redox signaling in cardiovascular pathophysiology: a focus on hydrogen peroxide and vascular smooth muscle cells, Redox Biol 9 (2016) 244–253.
[8] N.G. Milton, Role of hydrogen peroxide in the aetiology of Alzheimer's disease, Drugs Aging 21 (2004) 81–100.
[9] T.P. Szatrowski, C.F. Nathan, Production of large amounts of hydrogen peroxide by human tumor cells, Canc. Res. 51 (1991) 794–798.
[10] S.D. Lim, C. Sun, J.D. Lambeth, et al., Increased Nox1 and hydrogen peroxide in prostate cancer, Prostate 62 (2005) 200–207.
[11] T. Matoba, H. Shimokawa, K. Morikawa, et al., Electron spin resonance detection of hydrogen peroxide as an endothelium-derived hyperpolarizing factor in porcine coronary microvessels, Arterioscler, Thromb. Vasc. Biol. 23 (2003) 1224–1230.
[12] M. Zheng, P. Li, C. Yang, et al., Ferric ion immobilized on three-dimensional nanoporous gold films modified with self- assembled monolayers for electrochemical detection of hydrogen peroxide, Analyst 137 (2012) 1182–1189.
[13] H.M. Cochemé, A. Logan, T.A. Prime, et al., Using the mitochondria-targeted ratiometric mass spectrometry probe MitoB to measure H_2O_2 in living Drosophila, Nat. Protoc. 7 (2012) 946–958.
[14] V.V. Belousov, A.F. Fradkov, K.A. Lukyanov, et al., Genetically encoded fluorescent indicator for intracellular hydrogen peroxide, Nat. Methods 3 (2006) 281–286.
[15] T.Y. Cheng, J.W. Zhao, Z.Y. Wang, et al., A highly sensitive and selective hypochlorite fluorescent probe based on oxidation of hydrazine via free radical mechanism, Dyes Pigments 126 (2016) 218–223.
[16] X. Yang, Y. Guo, R.M. Strongin, Conjugate addition/cyclization sequence enables selective and simultaneous fluorescence detection of cysteine and homocysteine, Angew Chem. Int. Ed. Engl. 50 (2011) 10690–10693.
[17] J.W. Li, C.X. Yin, F.J. Huo, et al., Two high selective and sensitive ratiometric fluorescence probes for detecting hypochlorite, Sensor. Actuator. B Chem. 231 (2016) 547–551.
[18] X.F. Yang, M. Zhao, G. Wang, A rhodamine-based fluorescent probe selective for bisulfite anion in aqueous ethanol media, Sensor. Actuator. B Chem. 152 (2011) 8–13.
[19] H.J. Kim, C.H. Heo, H.M. Kim, Benzimidazole-based ratiometric two-photon fluorescent probes for acidic pH in live cells and tissues, J. Am. Chem. Soc. 135 (2013) 17969–17977.
[20] Y. Tang, J. Sun, B. Yin, A dual-response fluorescent probe for Zn^{2+} and Al^{3+} detection in aqueous media: pH-dependent selectivity and practical application, Anal. Chim. Acta 942 (2016) 104–111.
[21] Y.K. Yue, F.J. Huo, C.X. Yin, et al., Recent progress in chromogenic and fluorogenic chemosensors for hypochlorous acid, Analyst 141 (2016) 1859–1873.
[22] X.Q. Chen, F. Wang, J.Y. Hyun, et al., Recent progress in the development of fluorescent, luminescent and colorimetric probes for detection of reactive oxygen and nitrogen species, Chem. Soc. Rev. 45 (2016) 2976–3016.
[23] A.R. Lippert, G.C. Van de Bittner, C.J. Chang, Boronate oxidation as a bioorthogonal reaction approach for studying the chemistry of hydrogen peroxide in living systems, Acc. Chem. Res. 44 (2011) 793–804.
[24] M. Ren, B. Deng, J.Y. Wang, et al., A fast responsive two-photon fluorescent probe for imaging H_2O_2 in lysosomes with a large turn-on fluorescence signal, Biosens. Bioelectron. 79 (2016) 237–243.
[25] L. Du, N. Ni, M. Li, et al., A fluorescent hydrogen peroxide probe based on a 'click' modified coumarin fluorophore, Tetrahedron Lett. 51 (2010) 1152–1154.
[26] J.L. Han, C.Y. Chu, G.X. Cao, et al., A simple boronic acid-based fluorescent probe for selective detection of hydrogen peroxide in solutions and living cells, Bioorg. Chem. 81 (2018) 362–366.
[27] J. Nie, Y. Liu, J. Niu, et al., A new pyrene-based fluorescent probe with large Stokes shift for detecting hydrogen peroxide in aqueous solution and living cells, J. Photochem. Photobiol. Chem. 348 (2017) 1–7.
[28] X. Liang, X. Xu, D. Qiao, Dual mechanism of an intramolecular charge transfer (ICT)–FRET-based fluorescent probe for the selective detection of hydrogen peroxide, at al, Chem. Asian J. 12 (2017) 3187–3194.
[29] B.C. Zhu, H.L. Jiang, B.P. Guo, et al., A highly selective ratiometric fluorescent probe for hydrogen peroxide displaying a large emission shift, Sensor. Actuator. B Chem. 186 (2013) 681–686.
[30] J. Liu, J.J. Liang, C.L. Wu, et al., A doubly-quenched fluorescent probe for low-background detection of mitochondrial H_2O_2, Anal. Chem. 91 (2019) 6902–6909.
[31] W. Zhang, W. Liu, P. Li, et al., Rapid-response fluorescent probe for hydrogen peroxide in living cells based on increased polarity of C-B bonds, Anal. Chem. 87 (2015) 9825–9828.
[32] W.J. Zhang, F.J. Huo, Y.B. Zhang, et al., Mitochondria-targeted NIR fluorescent probe for reversible imaging H_2O_2/SO_2 redox dynamics in vivo, Sensor. Actuator. B Chem. 297 (2019) 126747.
[33] Y. Wen, F. Huo, C. Yin, A glycine spacer improved peptidyl-nuclear-localized efficiency for fluorescent imaging nuclear H_2O_2, Sensor. Actuator. B Chem. 296 (2019) 126624.
[34] Y. Wen, F. Huo, C. Yin, Organelle targetable fluorescent probes for hydrogen peroxide, Chin. Chem. Lett. 30 (2019) 1834–1842.
[35] Z. Mao, M. Ye, W. Hu, et al., Design of a ratiometric two-photon probe for imaging of hypochlorous acid (HClO) in wounded tissues, Chem. Sci. 9 (2018) 6035–6040.
[36] K. Gu, Y. Xu, H. Li, et al., Real-time tracking and in vivo visualization of beta-galactosidase activity in colorectal tumor with a ratiometric near-infrared fluorescent probe, J. Am. Chem. Soc. 138 (2016) 5334–5340.
[37] T.F. Brewer, G.B. Barragan, N. Wit, et al., A 2-aza-Cope reactivity-based platform for ratiometric fluorescence imaging of formaldehyde in living cells, Chem. Sci. 8 (2017) 4073–4081.
[38] Q.Q. Wan, S.M. Chen, W.S. Wan, et al., Lysosomal pH rise during heat shock monitored by a lysosome-targeting near-infrared ratiometric fluorescent probe, Angew Chem. Int. Ed. Engl. 53 (2014) 10916–10920.
[39] M.H. Lee, J.S. Kim, J.L. Sessler, Small molecule-based ratiometric fluorescence probes for cations, anions, and biomolecules, Chem. Soc. Rev. 44 (2015) 4185–4191.
[40] X.L. Wu, L.T. Zeng, B.Q. Chen, et al., A selective cascade reaction-based probe for colorimetric and ratiometric fluorescence detection of benzoyl peroxide in food and living cells, J. Mater. Chem. B. 7 (2019) 5775–5781.

[41] W.J. Zhang, T. Liu, F.J. Huo, et al., Reversible ratiometric fluorescent probe for sensing bisulfate/H_2O_2 and its application in zebrafish, Anal. Chem. 89 (2017) 8079–8083.
[42] Q.L. Xu, C.H. Heo, J.A. Kim, et al., A selective imidazoline-2-thione-bearing two-photon fluorescent probe for hypochlorous acid in mitochondria, Anal. Chem. 88 (2016) 6615–6620.
[43] Y.L. Pak, S.J. Park, Q. Xu, et al., Ratiometric two-photon fluorescent probe for detecting and imaging hypochlorite, Anal. Chem. 90 (2018) 9510–9514.
[44] Y.L. Pak, S.J. Park, D. Wu, et al., N-Heterocyclic carbene boranes as reactive oxygen species-responsive materials: application to the two-photon imaging of hypochlorous acid in living cells and tissues, Angew. Chem. Int. Ed. Engl. 6 (2018) 1567–1571.
[45] J. Matsui, M. Mitsuishi, T. Miyashita, A study on fluorescence behavior of pyrene at the interface of polymer Langmuir-Blodgett films, J. Phys. Chem. B 106 (2002) 2468–2473.
[46] P. Wang, K. Wang, Y. Gu, A highly selective fluorescent turn-on NIR probe for the bioimaging of hydrogen peroxide in vitro and in vivo, Sensor. Actuator. B Chem. 228 (2016) 174–179.
[47] D. Song, J.M. Lim, S. Cho, et al., A fluorescence turn-on H_2O_2 probe exhibits lysosome-localized fluorescence signals, Chem. Commun. 48 (2012) 5449–5451.
[48] X.J. Liu, H.H. Tian, L. Yang, et al., A sensitive and selective fluorescent probe for the detection of hydrogen peroxide with a red emission and a large Stokes shift, Sensor. Actuator. B Chem. 255 (2018) 1160–1165.
[49] Y.Z. Chen, X.M. Shi, Z.L. Lu, et al., A fluorescent probe for hydrogen peroxide in vivo based on the modulation of intramolecular charge transfer, Anal. Chem. 89 (2017) 5278–5284.
[50] Y. Wu, Z.Y. Li, Y.M. Shen, A novel ESIPT phthalimide-based fluorescent probe for quantitative detection of H_2O_2, ACS Omega 4 (2019) 16242–16246.
[51] K. Cheng, J.S. Lee, P. Hao, et al., Tetrazole-based probes for integrated phenotypic screening, affinity-based proteome profiling, and sensitive detection of a cancer biomarker, Angew Chem. Int. Ed. Engl. 56 (2017) 15044–15048.